

Quantum hall transformer in a quantum point contact over the full range of transmission

Stuart N. Thomas* and Jay D. Sau

Condensed Matter Theory Center and Joint Quantum Institute, Department of Physics,
University of Maryland, College Park, Maryland 20742-4111, USA

(Dated: June 25, 2024)

A recent experiment [Cohen *et al.*, Science **382**, 542 (2023)] observed a quantized $e^2/2h$ conductance tunneling into a fractional quantum hall edge in the strong coupling limit, which is consistent with the prediction of a quantum Hall transformer. We model this quantum point contact (QPC) as a quantum wire with a spatially-varying Luttinger parameter and a back-scattering impurity and use a numerical solution to find the wavepacket scattering and microwave (i.e. finite frequency) conductance at the interface. We then compare the microwave conductance to an analytic solution of a Luttinger liquid with an abruptly varying Luttinger parameter and a back-scattering impurity, which is obtained by mapping the problem to a boundary sine-Gordon (BSG) model. Finally, we show that the quantum Hall transformer can survive the inclusion of the domain wall that is expected to occur in a wide QPC, which is experimentally relevant, provided the momentum change in the QPC is generated by electrostatics. We find that back-scattering generated by the domain wall is of an order of magnitude consistent with the experiment.

Introduction.—Fractional quantum Hall (FQH) systems are one of the few experimentally known platforms that are expected to support chiral Luttinger liquid edge states [1]. Interestingly, a recent experiment [2] in graphene FQH quantum point contacts (QPCs) has seen differential conductance that closely matches theoretical predictions [3–5] (both low voltage and temperature power-law scaling as well as high voltage universality) based on the boundary sine-Gordon (BSG) model [6]. Such quantitative experiments, if described by the BSG, open more vistas into its physics, which can include rather intricate phenomena [6] accessed in relatively few experiments [7]. Interestingly, the high voltage universal regime of the BSG model, where the differential conductance is near a quantized value of $e^2/2h$ [2], realizes a dc voltage transformer, i.e. the quantum Hall transformer (QHT) [5].

Despite the agreement with the BSG model, the microscopic connection between this model and the experiment remain unclear. The interpretation of the BSG model as a tunneling term between chiral LL edges of $\nu = 1/3$ and $\nu = 1$ FQH states [3] is complicated by the irrelevance under the renormalization group [8] of such a perturbation and the large width of the QPC in experiments [2]. This raises the possibility that a more complex multi-tunneling model [9] as a model for the experiment. Similarly, a resonant impurity in the FQH state, which can realize such a strong tunneling [4], is also likely to depend on details, though resonances in the measured transmission [2] provide some motivation for this model.

A configuration for generically creating strong coupling [5] (i.e. the QHT limit), is in principle based on pinching the QPC to near the magnetic length and then

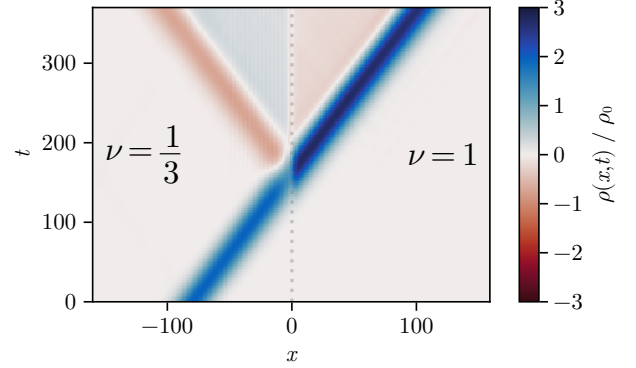


FIG. 1. Sign-flipping reflection of a charge wavepacket from the interface between $\nu = 1/3$ and $\nu = 1$ quantum Hall edge states, illustrating the quantum hall transformer behavior. The charge is normalized by a factor ρ_0 to illustrate the $2e^* \rightarrow -e^*$, $3e^* = e$ charge transfer. The constant charge near the interface at late times agrees with the sensitivity of the low frequency ac conductance to imperfections in the interface (see Fig. 2).

adiabatically varying the density between the two FQH states at filling $\nu = 1/3$ and $\nu = 1$. The adiabatic contact in this theory takes the form of a conventional Luttinger liquid with the Luttinger parameters adiabatically evolving between the values corresponding to $\nu = 1/3$ to $\nu = 1$. Since a weak back-scattering impurity is a relevant perturbation in an LL [8, 10], this model provides a natural framework to describe a high-temperature/voltage limit with a differential conductance of $e^2/2h$ and a low temperature impurity dominated limit with vanishing differential conductance. However, whether such a model can describe the experiment [2], which is not in the narrow QPC limit, is also unclear.

In this work, we provide an alternative (relative to

* snthomas@umd.edu

Ref. 3) interpretation of the BSG model [6]—as arising from an impurity in the above Luttinger liquid model [5]—to understand the quantitative conductance in the weak and strong impurity limit. We do this by comparing the numerically computed ac conductance of a model of a Luttinger liquid with an impurity and a spatially varying Luttinger parameter to the ac conductance of the BSG model. This allows us to relate the effective back-scattering in the BSG model with the microscopic parameters in the Luttinger model. Finally, we discuss models of a wide QPC that can be described by the Luttinger model where the scattering from the domain wall can provide the back-scattering in the BSG.

Luttinger liquid model.—The Hamiltonian for an impurity in a Luttinger liquid [8], assuming the density variation back-scattering [10] to be of strength g at $x = 0$, can be represented by the Hamiltonian

$$H = \int dx \frac{v(x)}{2\pi} [K(x)\Pi^2 + K(x)^{-1}(\partial_x\phi)^2] - g \cos 2\phi(0), \quad (1)$$

where the boson field ϕ is defined in terms of the charge density $\rho = -\pi^{-1}\partial_x\phi$ in units of the electron charge e . Here $\Pi(x)$ is the momentum that is canonically conjugate ($[\phi(x), \Pi(x')] = i\pi\delta(x-x')$) to the boson field $\phi(x)$. The pair of edges of a FQH strip at filling fraction ν has a Luttinger parameter $K(x) = \nu$ and a mode velocity $v(x)$ that matches the edge velocity, which we take to be 1 across the junction by rescaling x [3]. To represent the junction, we smoothly vary $K(x)$ in space. Conservation of charge requires that the current operator is written as $j = \pi^{-1}\partial_t\phi = (i/\pi)[H, \phi] = vK\Pi/\pi$. An applied voltage V can be described by adding a perturbation $H_{\text{ext}} = V\phi(0)$ to the Hamiltonian H .

In the absence of back-scattering (i.e. $g = 0$), which is referred to as the quantum Hall transformer [5], the Hamiltonian in Eq. 1 is harmonic so that the conductance is independent of temperature. By approximating the $K(x)$ profile as exponential over a region of width d and constant otherwise, and using the Kubo formula for the response of the current $j(\omega)$ with perturbation $V(\omega)$, the ac conductivity is analytically solvable, yielding

$$G(\omega) = \frac{e^2}{h} \frac{e^{-i\theta} \sqrt{K_- K_+}}{\cosh \Delta - i(\theta/\Delta) \sinh \Delta} \quad (2)$$

where $\Delta^2 = (\frac{1}{2} \log K_-/K_+)^2 - \theta^2$ and $\theta = \omega d/v$. The value of θ parameterizes the width of the junction d relative to the wavelength of the driven modes. This formula reduces to the quantum hall transformer dc conductivity $G \sim (2e^2/h)(K_-^{-1} + K_+^{-1})^{-1}$ [5, 9] as ω goes to 0 but approaches $G \sim (e^2/h)(K_- K_+)^{1/2}$ in the large frequency/long junction limit ($\omega \gg v/d$). The $e^2/2h$ dc conductance in this limit can be understood as the Andreev reflection-like process (see Fig. 1) where a charge packet of charge $2e/3$ is reflected to a packet of $-e/3$ with the opposite sign. This process can be understood to be

a result of the conservation of chiral charge in the Luttinger liquid [11] in the absence of back-scattering since the chiral charge of the incoming and reflected packets are $K_-^{-1}(2e/3) = 2e$ and $K_-^{-1}(e/3) = e$ respectively while the transmitted packet has a chiral charge of $K_+^{-1}e = e$.

Numerical model ac conductance.—The above result in the dc limit ($\omega \rightarrow 0$) is fine-tuned to $g = 0$, since a finite strength of impurity $g > 0$ is expected to be a relevant perturbation [8] and requires a numerical treatment. For this purpose, we approximate the model in Eq. 1 as an interacting fermion lattice model with next-nearest neighbor interactions [12], described by a Hamiltonian

$$H = \sum_n (t_n c_n^\dagger c_{n+1} + \text{h.c.} - \mu_n n_n + U_n n_n n_{n+1} + U'_n n_n n_{n+2}) + u n_0 \quad (3)$$

where the spatially dependent parameters correspond to $K = 1$ and $K = 1/3$ Luttinger liquids with a short, smooth interface. For the $K = 1$ side we use $t_n = 0.308$, $\mu_n = 0.360$, $U = 0$ and $U'_n = 0$ while for the $K = 1/3$ side we use $t_n = 0.122$, $\mu_n = 0.293$, $U = 0.293$ and $U'_n = 0.439$. This choice keeps the velocity and background magnetization approximately constant. The interface between the two sides consists of a smooth 3-site transition in each of the parameters and a single-site barrier u . Such a model can be transformed to a spin-1/2 XXZ model via a Jordan-Wigner mapping.

We can probe the ac conductance of this junction using a Gaussian chiral wavepacket, generated by a local quench in the chemical potential μ_n and a gauge field a_n such that $t_n \mapsto t_n e^{ia_n}$ [13]. We use the density matrix renormalization group [14, 15] to solve for the ground state of this quenched Hamiltonian and then use the time-evolving block decimation algorithm [16, 17] to evolve the packet in real time with a fourth-order Trotter decomposition [18]. The propagation of these packets is nearly dissipationless, since the packet is perturbatively small ($\rho \lesssim 10^{-3}$), and the transport process is clear from the the packet transmission, as shown in Fig. 1. Comparing the initial and transmitted packet in the frequency domain gives the ac conductance, plotted in Fig. 2. Note that due to the discrete geometry and the finite bandwidth of the Gaussian wavepacket, there is a trade-off between frequency range and resolution, and therefore two different packet widths are used. Numerical details can be found in the Supplementary Material (SM).

Boundary sine-Gordon model.—The Hamiltonian Eq. 1, for $g > 0$, is essentially an impurity in a Luttinger liquid, which can be solved by mapping to a boundary sine-Gordon model (BSG) [6] by folding the $x < 0$ solution using a reflection $x \rightarrow -x$ [19]. Applying this transformation generates a two-component boson field $\phi_-(x) = \phi(-x)$ and $\phi_+(x) = \phi(x)$ for $x \geq 0$. The effect of a weak impurity g is expected to be limited to low energy modes, whose wavelength is longer than the vari-

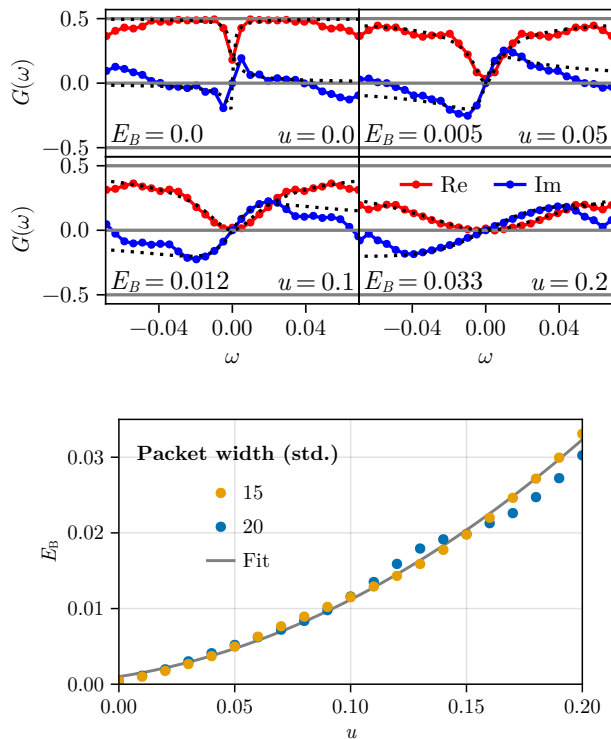


FIG. 2. **(top)** ac conductivity for various impurity strengths u and packet width 15 demonstrating near $G = e^2/2h$ for $u = 0$. The real part of the data is fit to Eq. 12 to calculate barrier energy E_B , with fits shown as dashed lines. **(bottom)** Fit value of E_B as a function of impurity strength u , demonstrating a quadratic relationship. Data from the narrower packet is fit to $E_B = A(u + u_0)^2$, which yields $A = 0.55$ and $u_0 = 0.04$, the latter of which represents the intrinsic back-scattering of the Luttinger parameter crossover.

ation of $K(x)$. We will therefore assume the Luttinger parameter associated with ϕ_{\pm} to be constants K_{\pm} respectively. The boundary condition for $\phi_{\pm}(x \sim 0)$ changes abruptly near $x \sim 0$, so that the boundary condition is written as $K_+^{-1} \partial_x \phi_+ = -K_-^{-1} \partial_x \phi_-$.

This boundary condition couples the otherwise decoupled left and right channels. The fields decouple completely under a rescaling by $K_{\pm}^{-1/2}$ and an $O(2)$ rotation, with ξ and $\bar{\xi}$ fields defined as

$$\begin{pmatrix} \xi \\ \bar{\xi} \end{pmatrix} = \Gamma \begin{pmatrix} K_-^{-1/2} & K_+^{-1/2} \\ K_+^{-1/2} & -K_-^{-1/2} \end{pmatrix} \begin{pmatrix} \phi_- K_-^{-1/2} \\ \phi_+ K_+^{-1/2} \end{pmatrix}. \quad (4)$$

and likewise with their conjugate momenta η and $\bar{\eta}$ (rescaling by $K_{\pm}^{1/2}$ instead of $K_{\pm}^{-1/2}$). Here $\Gamma \equiv (K_-^{-1} + K_+^{-1})^{-1/2}$. Under this transformation, the boundary conditions become $\xi(0) = 0$ and $\partial_x \xi(0) = 0$.

Since ξ vanishes at $x = 0$, the original field at the boundary $\phi(0)$ can be written purely in terms of $\xi(0)$ as $\phi(0) = \Gamma \xi(0)$, decoupling ξ from $\bar{\xi}$. The $\bar{\xi}$ equation has no boundary term and cannot affect the current, so we

focus on the ξ part of the Hamiltonian:

$$H_{\xi} = \int_0^{\infty} \frac{dx}{2\pi} [\eta^2 + (\partial_x \xi)^2] - g \cos(2\Gamma \xi(0)). \quad (5)$$

Writing the perturbation H_{ext} to the Luttinger liquid Hamiltonian Eq. 1 in terms of $\xi(0)$, we conclude that the voltage V transforms to an effective voltage $V_{\text{eff}} = \Gamma V$ applied to the Hamiltonian H_{ξ} . The total current flowing through the junction then transforms into

$$j = \Gamma \pi^{-1} \eta(0). \quad (6)$$

To analyze the above semi-infinite systems we combine the fields $\xi(x)$ and $\eta(x)$ into the chiral boson field $\xi_c(x) = (1/2)[\xi(|x|) + \int_0^x dx' \eta(|x'|)]$ on the entire real line $x \in (-\infty, \infty)$ [20]. The von Neumann boundary conditions $\partial_x \xi(0) = 0$ ensure that $\xi_c(x)$ is differentiable at $x = 0$. Following Refs. 21 and 22, and introducing a soft UV cutoff a we refermionize the bosonic Hamiltonian by defining the chiral fermion field

$$\psi_c(x) = \frac{\alpha}{\sqrt{2\pi a}} e^{-2i\xi_c(x)}, \quad (7)$$

where $\alpha = \exp[i\pi(\xi_c(0) - \xi_c(\infty))]$ is the fermion parity of the refermionized model. The boundary term, for the specific case $\Gamma = 1/2$ (corresponding to $K_+ = 1/3$ and $K_- = 1$), can be written in terms of this chiral fermion operator as

$$g \cos \xi(0) = \sqrt{2E_B} \alpha \left(\psi_c(0) + \psi_c^{\dagger}(0) \right) \quad (8)$$

where $E_B = g^2 \pi a / 4$. This term is quadratic in fermion operators due to the operator α .

The equations of motion of the fermion fields $\psi_c(x)$ and α resulting from the above boundary Hamiltonian results in Andreev transmission [23] of $\psi_c(x)$ from the operator α which behaves like a Majorana operator.

However, the charge of the chiral fermion ψ_c does not correspond to electronic charge. This issue is resolved by defining the fermion in the original interval $x \in [0, \infty]$ in terms of the chiral fermions using the relation

$$\psi^{\dagger}(x) = e^{ik_F x} \psi_c^{\dagger}(x) + e^{-ik_F x} \psi_c(-x). \quad (9)$$

By using this definition of the fermion operator, we can write the current in Eq. 6 as:

$$j(x) = (i/2)(\psi^{\dagger}(x) \partial_x \psi(x) - \text{h.c.}), \quad (10)$$

which is the conventional form of the fermion current in a one dimensional wire. Here the wavelength for the chiral fields is assumed to be much longer than $k_F^{-1} = 1$ (chosen to be consistent with Fermi velocity and mass being one). Using the fermion definition Eq. 9 with the corrected charge, the Andreev and normal scattering amplitudes for the fermion $\psi(x)$ can be computed from the Bogoliubov-de Gennes equations (see SM for details),

similar to resonant Andreev reflection from a Majorana zero mode [23]:

$$r_A = \frac{iE}{iE + E_B} \quad r_N = -\frac{E_B}{iE + E_B}. \quad (11)$$

At low energies $|E| \ll |E_B|$ we see that $|r_N| \sim 1$ (i.e. perfect normal reflection) while high energy fermions with $|E| \gg |E_B|$, are Andreev reflected (i.e. $|r_A| \sim 1$).

This result is consistent with previous works solving Eq. 5 using a Kramers-Wannier duality [24, 25] and conformal field theory techniques [6, 26, 27].

The voltage and temperature dependence resulting from this Andreev reflection [9, 23] is in good agreement with recent experimental results [2]. Applying the formalism of dynamic conductance [28], we find the ac conductance associated with the above Andreev reflection process to be:

$$G(\omega) = \frac{e^2}{2h} \left[1 - \frac{E_B}{i\omega} \text{Ln} \left(1 + \frac{i\omega}{E_B} \right) \right]. \quad (12)$$

The real part of the ac conductance vanishes as $\omega \rightarrow 0$, which is consistent with the irrelevance of the tunneling perturbation [8]. Furthermore, it reaches the harmonic value of $1/2$ as $\omega \rightarrow \infty$, which is consistent with Eq. 2 when $v/d \gg \omega \gg E_B$. We fit the ac conductances in Fig. 2 with Eq. 12 and find a close resemblance at low frequencies, where the ratio of Gaussians is well defined. Furthermore, we can deduce the values of E_B for difference back-scattering strengths g , which is seen in Fig. 2 to be broadly consistent with the theoretical estimate apart from a shift u_0 that likely arises from the spatial variation of $K(x)$.

Luttinger liquid as a model for the QPC.— The Luttinger liquid model Eq. 1 for the quantum Hall transformer, which is based on the edge charges and currents, was originally justified for a QPC of width comparable to the magnetic length l_B [5], however this justification must be modified for the relevant experimental realization [2] where the QPC is much wider than a magnetic length. This is, however, subtle when the filling varies between the values of $\nu_- = 1$ and $\nu_+ = 1/3$ in the middle of the QPC, resulting in a compressible domain wall shown in Fig. 3. While a detailed analysis of the low-energy structure based on numerical diagonalization or Chern-Simons theory [29] of the QPC is beyond the scope of the current work, for QPC widths smaller than $W \lesssim v_{\text{DW}}/k_B T_0$ and $v_{\text{DW}}/V_{\text{bias}}$, the domain-wall modes would effectively be gapped on a scale that is larger than the temperature T_0 and the applied bias V_{bias} , scaling with the velocity v_{DW} of domain-wall excitations. One can then expect the charge dynamics to be dominated by the edges of the QPC (see the SM for more details) such that the Luttinger liquid model is a reasonable description.

The quantum Hall transformer behavior in the conductance of the harmonic Luttinger liquid model—as proposed in Ref. 5—can be attributed to momentum-based

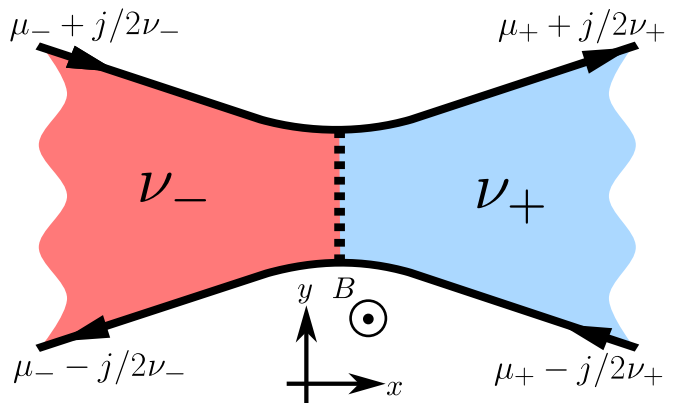


FIG. 3. Schematic of a QPC between filling $\nu_- = 1$ and $\nu_+ = 1/3$. The arrows represent the direction of movement of the electron at each edge. The dotted line represents a domain wall with effective chiral charge $\nu_- - \nu_+ = 2/3$ with disorder [30]. The chemical potential of each segment of edge is shown to be $\mu_{\pm} + \text{sgn}(y)j/2\nu_{\pm}$ where j is the total current flowing through the QPC and the edge velocity near the ends is chosen to be unity.

chiral charge conservation [11]. Motivated by this argument, we explicitly consider the effect of momentum conservation to a model of the QPC with a short domain wall dominated by edge charges as shown in Fig. 3. We choose the chemical potentials of the edges to be $\mu_{\pm} \pm j/2\nu_{\pm}$ on the left-hand side of the QPC and $\mu_{\pm} \pm j/2\nu_{\pm}$ on the right side. Here j is the current flowing through the QPC and ν_{-}, ν_{+} are the filling factors on the two sides. Assuming that the QPC does not generate significant noise as in the two extremes of the Luttinger liquid, the rate at which canonical momentum is carried away by the current (i.e. the total force in the x -direction) is simply a product of the current on each edge and the corresponding vector potential and is written as

$$F_{\text{current}} = (\nu_- \mu_- - \nu_+ \mu_+) BW'. \quad (13)$$

In the above equation, the gauge is chosen so that the vector potential at the ends of the top and bottom edges in Fig. 3 is $A = \pm BW' \hat{x}/2$, the edge velocity at the ends is chosen to be unity and W' is the width of the QPC at the left and right ends of Fig. 3 where μ_{\pm} are measured. This momentum change is generated by the interaction of the charge density with the electrostatic potential generated by the gates, generating a force $F_{\text{gates}}(\mu_{-}, \mu_{+}, j)$. Within linear response, one can expand this force in terms of $\delta\mu \equiv (\mu_{+} - \mu_{-})/2$ and j as $F_{\text{gates}}(\mu_{-}, \mu_{+}, j) = C_0 + C_1 \delta\mu + C_2 j$ where the coefficients can depend on $\bar{\mu} \equiv (\mu_{+} + \mu_{-})/2$. The current j can be determined from the momentum conservation equation

$$C_0 + C_1 \delta\mu + C_2 j - (\nu_- \mu_- - \nu_+ \mu_+) BW' = 0. \quad (14)$$

Since momentum conservation must apply in equilibrium (i.e. $\mu_- = \mu_+$ and $j = 0$), the constant term but be

$C_0 = (\nu_- - \nu_+) \bar{\mu} B W'$. For the special case of a QPC with mirror symmetry along the y axis, we can use the mirror operator to interchange the chemical potentials on the top and bottom edges without changing the direction of the currents so that this transformation flips j and preserves μ_{\pm} . Applying this symmetry to Eq. 14, leads to the conclusion that $C_2 = 0$, which then forces the constraint $\mu_+ = \mu_-$. The voltage in the QPC is the difference in the chemical potentials of the two incoming leads is $V = j(1/2\nu_- + 1/2\nu_+)$, which results in the expected conductance of the quantum Hall transformer matching $G = 2\nu_- \nu_+ / (\nu_- + \nu_+)$ [5]. This result is explicitly demonstrated for an edge model of the QPC in the SM. The quantum Hall transformer conductance is reduced by impurity-induced large momentum elastic back-scattering. As elaborated in the SM, we find that scattering from a soliton-like structure (e.g. $\nu = 2/3$ domain wall) can support a scattering matrix element in Eq. 1 that is of the correct order of magnitude to account for the recent measurements [2].

Conclusion.— We have provided an alternative interpretation to the BSG model that is used to fit the recent experiments [2] as arising from an impurity in the Luttinger model for the QHT [5]. We have compared these results with a numerical solution of the Luttinger model to map out the correspondence between the parameters of the two models. These results also make predictions for the microwave conductivity in addition to previous results [3, 9, 25] on shot noise that could guide future studies on these QPC systems. In addition, we have shown that inclusion of momentum conservation in the dynamics of the domain wall that would likely form in the QPC can be consistent with the Luttinger liquid description both in terms of the QHT as well as impurity back-scattering. Extending this model to include more microscopic details for example using a Chern-Simons mean-field treatment of the QPC [29] would be an interesting future direction.

We thank Bertrand Halperin, Michael Zaletel and Andrea Young for valuable discussion. S.T. thanks the Joint Quantum Institute at the University of Maryland for support through a JQI fellowship. J.S. acknowledges support from the Joint Quantum Institute. This work is also supported by the Laboratory for Physical Sciences through its continuous support of the Condensed Matter Theory Center at the University of Maryland.

[1] A. M. Chang, *Reviews of Modern Physics* **75**, 1449 (2003).

- [2] L. A. Cohen, N. L. Samuelson, T. Wang, T. Taniguchi, K. Watanabe, M. P. Zaletel, and A. F. Young, *Science* **382**, 542 (2023).
- [3] N. P. Sandler, C. d. C. Chamon, and E. Fradkin, *Physical Review B* **57**, 12324 (1998).
- [4] C. L. Kane, Resonant tunneling between quantum hall states at filling $\nu = 1$ and $\nu = 1/3$ (1998), arXiv:cond-mat/9809020 [cond-mat.mes-hall].
- [5] D. B. Chklovskii and B. I. Halperin, *Physical Review B* **57**, 3781 (1998).
- [6] P. Fendley, H. Saleur, and N. P. Warner, *Nuclear Physics B* **430**, 577 (1994).
- [7] A. Anthore, Z. Iftikhar, E. Boulat, F. Parmentier, A. Cavanaugh, A. Ouerghi, U. Gennser, and F. Pierre, *Physical Review X* **8**, 031075 (2018).
- [8] C. Kane and M. P. Fisher, *Physical Review B* **46**, 15233 (1992).
- [9] C. d. C. Chamon and E. Fradkin, *Physical Review B* **56**, 2012 (1997).
- [10] N. Sedlmayr, J. Ohst, I. Affleck, J. Sirker, and S. Eggert, *Physical Review B* **86**, 121302 (2012).
- [11] S. Wang and J. D. Sau, arXiv preprint arXiv:2401.09409 (2024).
- [12] T. Giamarchi, *Quantum physics in one dimension*, Vol. 121 (Clarendon press, 2003).
- [13] M. Ganahl, E. Rabel, F. H. Essler, and H. G. Evertz, *Physical review letters* **108**, 077206 (2012).
- [14] S. R. White, *Physical Review Letters* **69**, 2863 (1992).
- [15] S. R. White, *Physical Review B* **48**, 10345 (1993).
- [16] G. Vidal, *Physical Review Letters* **91**, 147902 (2003).
- [17] G. Vidal, *Physical Review Letters* **93**, 040502 (2004).
- [18] T. Barthel and Y. Zhang, *Annals of Physics* **418**, 168165 (2020).
- [19] P. Fendley, A. Ludwig, and H. Saleur, *Physical Review B* **52**, 8934 (1995).
- [20] M. Fabrizio and A. O. Gogolin, *Physical Review B* **51**, 17827 (1995).
- [21] R. Shankar, in *Low-Dimensional Quantum Field Theories for Condensed Matter Physicists* (World Scientific, 1995) pp. 353–387.
- [22] J. Von Delft and H. Schoeller, *Annalen der Physik* **510**, 225 (1998).
- [23] M. Wimmer, A. Akhmerov, J. Dahlhaus, and C. Beenakker, *New Journal of Physics* **13**, 053016 (2011).
- [24] F. Guinea, *Physical Review B* **32**, 7518 (1985).
- [25] N. P. Sandler, C. d. C. Chamon, and E. Fradkin, *Physical Review B* **59**, 12521–12536 (1999).
- [26] S. Ghoshal and A. Zamolodchikov, *International Journal of Modern Physics A* **09**, 3841–3885 (1994).
- [27] M. Ameduri, R. Konik, and A. LeClair, *Physics Letters B* **354**, 376 (1995).
- [28] M. Büttiker, A. Prêtre, and H. Thomas, *Physical review letters* **70**, 4114 (1993).
- [29] A. Lopez and E. Fradkin, *Physical Review B* **44**, 5246 (1991).
- [30] C. Kane, M. P. Fisher, and J. Polchinski, *Physical review letters* **72**, 4129 (1994).

Supplementary Material for “Exact Andreev reflections from impurities in quantum Hall point contacts and Luttinger liquids”

Stuart N. Thomas and Jay D. Sau
(Dated: June 25, 2024)

NUMERICAL DETAILS

The $K = 1/3$ Luttinger liquid poses a challenge to simulate numerically since there is no explicit form for the parameters in Eq. 3 of the main text which lead to such a scaling coefficient. To calculate the corresponding parameters numerically, we measure the Drude weight and the compressibility and relate them back to the Luttinger parameters as $D = Kv/2\pi$ and $\chi = K/\pi v$. We use the VUMPS algorithm [1] to determine these quantities for infinite systems to remove finite-size effects, particularly in calculating the compressibility. The Luttinger parameter is first set by optimizing the ground state ψ over $K^2(\psi) = 2\pi^2 D(\psi)\chi(\psi)$. Then, the velocity is tuned by rescaling t_n and μ_n . We use a large field to avoid the gapped phase near $\mu_n = 0$ when $U_n > 0$. We find that $t_n = 0.122$, $U = 0.293$, $U'_n = 0.439$ and $\mu_n = 1.22$ gives parameters of $v = 0.5^1$ and $K = 0.332$. To match the magnetization and velocity on the $K = 1$ side, we set the hopping to $t_n = 0.308$ and the chemical potential to $\mu_n = (4t_n^2 - v^2)^{1/2} = 0.360$.

We represent the interface between these two phases as a slow variation of $K(x)$ relative to the lattice spacing, which corresponds to slow variations in the lattice parameters. The Hamiltonian in Eq. 3 of the main text can be transformed by a Jordan-Wigner transformation to an XXZ Hamiltonian.

Introducing smooth variations of μ_n and a_n can be used to generate wavepackets of chiral charge to numerically simulate scattering in the lattice fermion model [2, 3]. To understand this, we first apply a gauge transformation (i.e. time-dependent unitary transformation) to set $\mu_n = 0$ and transform $\tilde{a}_n(t) = a_n - \int_{-\infty}^t d\tau (\mu_{n+1} - \mu_n)$. In the continuum limit where \tilde{a}_n is slowly varying, the field is Lorentz invariant so that a variation $\tilde{a}_n = f(vt - n)$ is Lorentz invariant. In fact, such a vector potential represents a wavepacket of chiral charge that propagates with velocity v . We can apply a gauge transformation so that $\partial_t a_n|_{t=0} = 0$ and we get $\mu_n = \sum_{m < n} f'(t - m)$ and $a_n = f(t - n)$. In our simulations, we use a Gaussian for $f(x)$. To generate Figs. 1 and 2 of the main text, we run simulations on a 640 site system with a 3 site crossover region. We use a Trotter step size of $\tau = 2$ which we find is sufficient due to the slow dynamics.

REFERMIONIZATION DETAILS

To formalize the refermionization procedure in accordance with Ref. 4, we consider the fields $\xi(x)$ and $\eta(x)$ on the finite wire $x \in (0, L)$. In this case, we can expand each as a Fourier series

$$\begin{aligned}\xi(x) &= A_0 + \sqrt{2} \sum_{n=1} A_n e^{\pi n a/L} \cos \frac{\pi n x}{L} \\ \eta(x) &= B_0 + \sqrt{2} \sum_{n=1} B_n e^{\pi n a/L} \cos \frac{\pi n x}{L}\end{aligned}$$

where only cosine terms are included since $x > 0$ and where a is a soft UV cutoff for the coefficients A_n and B_n . From the canonical commutation relation $[\xi(x), \eta(x')] = i\pi\delta(x - x')$, we find

$$\begin{aligned}[A_m, B_n] &= \frac{\pi i}{L} e^{-2\pi n a/L} \delta_{mn} \\ (a \rightarrow 0) &= \frac{\pi i}{L} \delta_{mn}.\end{aligned}$$

The chiral field $\xi_c(x) = (1/2)[\xi(|x|) + \int_0^x dx \eta(|x|)]$ becomes

$$\xi_c(x) = \frac{A_0}{2} + \frac{B_0 x}{2} + \frac{1}{\sqrt{2}} \sum_{n=1} e^{-\pi n a/L} \left[A_n \cos \frac{\pi n x}{L} + \frac{B_n L}{\pi n} \sin \frac{\pi n x}{L} \right]$$

¹ We choose $v = 0.5$ instead of $v = 1$ to access smaller frequencies without increasing the wavelength.

which obeys

$$\begin{aligned} [\xi_c(x), \xi_c(x')] &= -\frac{i}{2} \sum_{n=-\infty}^{\infty} \tan^{-1} \left(\frac{x - x' - 2nL}{a} \right) \\ (a \rightarrow 0) &= -\frac{i\pi}{4} \operatorname{sgn}(x - x'). \end{aligned}$$

This relation lacks the $O(1/L)$ term found in Ref. 4 due to the inclusion of the zero modes A_0 and B_0 . These zero modes become the Klein factor and $\exp(2\pi Nx/L)$ factors in the bosonization identity of Ref. 4.

The Hamiltonian in Eq. 5 of the main text then becomes

$$H_\xi = \int_0^L \frac{dx}{\pi} (\partial_x \xi_c(x))^2 + g \cos 2\xi_c(0). \quad (1)$$

In the noninteracting limit ($g = 0$), the equation of motion becomes $\partial_t \xi_c = \partial_x \xi_c$, demonstrating that $\xi_c(x)$ is in fact chiral.

One subtlety in this refermionization procedure is that $\xi(x)$ and $\eta(x)$ are not well-defined operators on the Hilbert space of states. This concern was mentioned in Ref. 4 and remedied with explicit Klein factors. Consider for example the unitary transformation $T = \exp(2\pi iN)$ where $N = \pi^{-1} \int_0^L dx \eta(x) = B_0 L/\pi$ is the chiral fermion number. Since $[N, \xi(x)] = i$, the transformed field is $T\xi(x)T^\dagger = \xi(x) + 2\pi$ which leads to the equivalence $A_0 \equiv A_0 + 2\pi$. In essence, the operator A_0 is periodic and only defined on a compact subspace. Since our refermionization prescription (Eq. 7 of the main text) only depends on A_0 only up to this transformation, the fermion field ψ_c is well-defined. In other words, we do not utilize expressions of the form $\exp(ic\xi_c(x))$ where $c \notin \mathbb{Z}$.

ANDREEV REFLECTION

The transmission due to the interaction term in Eq. 8 on the main text can be solved by solving the time evolution of $\gamma_1(x)$ and α using the Heisenberg equation of motion in the frequency domain:

$$\begin{aligned} \omega \gamma_1(x) &= -[H_{\gamma_1}, \gamma_1(x)] \\ &= i\partial_x \gamma_1(x) - 2\sqrt{2E_B} \alpha \delta(x), \\ \omega \alpha &= -[H_{\gamma_1}, \alpha] \\ &= 2\sqrt{2E_B} \gamma_1(x). \end{aligned}$$

Integrating the region around $x = 0$ gives

$$\begin{aligned} \gamma_1(0_+) - \gamma_1(0_-) &= i\sqrt{2E_B} \alpha \\ \gamma_1(0_+) + \gamma_1(0_-) &= \frac{2\omega}{\sqrt{2E_B}} \alpha. \end{aligned}$$

The transmission coefficient is

$$\begin{aligned} T &= \gamma_1(0_+)/\gamma_1(0_-) \\ &= \frac{\omega + iE_B}{\omega - iE_B} \end{aligned}$$

which is a pure phase. Transforming back to the fermion basis, we calculate the transmission matrix of ψ_c to be

$$t_0 = \frac{1}{iE + E_B} \begin{pmatrix} -E_B & iE \\ iE & -E_B \end{pmatrix}.$$

Refolding this system using Eq. 9 of the main text, this transmission matrix leads to a reflection matrix of

$$\begin{aligned} r &= \sigma_x t_0 \\ &= \frac{1}{iE + E_B} \begin{pmatrix} iE & -E_B \\ -E_B & iE \end{pmatrix} \end{aligned}$$

which leads to the amplitudes in Eq. 11 of the main text.

REVIEW OF NOISE

Using Eq. 11 we can reproduce known formulae for the conductance and shot noise [5–7], the latter of which reveals Andreev reflection in the form of the charge of the scattered observables [8, 9]. The noise at high voltages $V \gg E_B$ goes as $P \propto E_B \ll I \sim V/2$ resulting from incoherent normal reflection caused by the impurity that would vanish in the absence of backscattering. Furthermore, the noise power nearly vanishes relative to the current as a result of most of the current being carried by perfect Andreev reflection. In this case, the noise power approaches $P \sim \pi e^2 E_B / 2h \sim \delta I$ where δI is the small back-scattered component of the current at high voltages. The effective charge of the back-scattered current is $P/2\delta I \sim e/2$. On the other hand at low voltages the power goes as $P \sim V^3/12E_B^2 \sim 2I$, which is consistent with tunneling of electrons as expected from the fraction at $\nu = 1$. This is because the effective charge $P/2\delta I \sim e$, which is twice the high voltage value. This is similar to tunneling in superconductors where the high voltage noise from quasiparticles is twice the result from Cooper pair tunneling at low voltages.

The asymptotic behavior of the shot noise is plotted in Fig. 1.

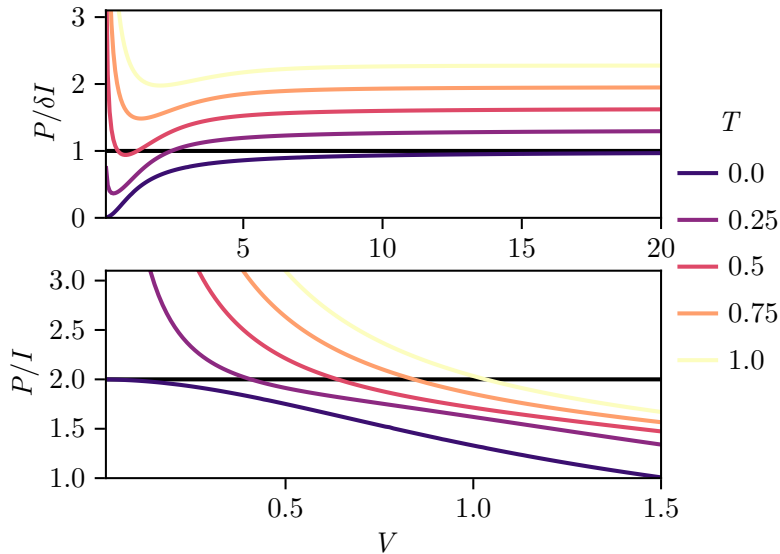


FIG. 1. Asymptotic behavior of noise P representing $V \rightarrow \infty$ (top) and $V \rightarrow 0$ (bottom) asymptotic behavior. The $T = 0$ case matches $P \rightarrow \delta I$ in the large voltage limit and $P \rightarrow 2I$ in the small voltage limit. The impurity energy is $E_B = 1$.

MODEL FOR QPC WITH A QUANTUM HALL TRANSFORMER

Here we discuss a possible model for a QPC that is wider than the magnetic length so that there is a segment of domain-wall across the QPC. The QPC has 5 segments of chiral fractional quantum Hall edges. The density $\rho(s, t)$ on each of the edges, which are the only compressible regions in the QPC, is written as

$$\partial_t \rho - \partial_s [v(s)\rho(s)] = \nu \partial_s \phi(s), \quad (2)$$

where s is a coordinate along the relevant edge segment, $v(s)$ is the edge velocity, ν is the effective filling factor of the edge and $\phi(s)$ is the electrostatic potential of the device. The edge current is $v(s)\rho(s)$, while the RHS represents an anomaly contribution from the bulk quantum Hall conductance. For a steady state system, as is relevant for computing conductivity, this implies

$$v_a(s)\rho_a(s) + \nu_a(s)\phi_a(s) = \mu_a(s)\nu_a(s) = \text{constant} \quad (3)$$

over a certain segment of edge labelled by a . For the four segments of physical edges of the QPC, the label $a = (t/b, \pm)$ corresponding to the top and bottom edges of the QPC in Fig. 3 (main text) and \pm referring to the sign of the coordinate s with $s = 0$ referring to the position of the domain-wall. In this notation, $\nu_a = \nu_{\pm}$ depending on filling

fraction of the adjacent bulk for $s > 0$ or $s < 0$. Referring to Fig. 3 and keeping in mind current conservation the chemical potentials μ_a for the four edges of the QPC are $\mu_a = \mu_{\pm} \pm j/2\nu_{\pm}$. For the dotted domain-wall the effective filling factor is $\nu = \nu_- - \nu_+$, though this value only represents the charged mode; the neutral mode [10] is not shown in the diagram. The value of the constant on each edge depends on the chemical potential at each edge which is determined by local current conservation at the junctions [11]. The electrostatic potential $\phi(r)$ is determined from the total charge density $\rho(r)$ through

$$\phi(r) = \phi_{\text{ext}}(r) + \int d^2r' U(r-r')\rho(r'), \quad (4)$$

where the two dimensional coordinate r includes both the bulk and edges of the QPC as well the domain-wall.

For simplicity, we will consider the limit where the domain-wall edge mode velocity and string tension T_S is large enough to make the domain-wall density of states and displacement from the narrowest point small. This assumption makes the domain-wall contribution to the total charge negligible and is equivalent to the assumption about edge dominance made in the main text. The above equation for the electrostatic potential can now be decomposed into edge contributions

$$\phi_a(s) = \phi_{\text{ext},a}(s) + \int ds' \sum_b U_{ab}(s,s')\rho_b(s'). \quad (5)$$

Using Eq. 3 this equation can be rewritten as

$$\int ds' \sum_b \left[U_{ab}(s,s') + \frac{\delta(s-s')\delta_{ab}v_a(s)}{\nu_a(s)} \right] \rho_b(s') = \mu_a - \phi_{\text{ext},a}(s), \quad (6)$$

which is a well-defined inversion of a positive-definite symmetric matrix for $\rho_b(s)$.

The negligible bias dependence of the density near the QPC implies that the electric field cannot contribute momentum change near the domain wall. This implies that the change in canonical momentum of the edge carriers resulting from charge leaving and entering the top and bottom ends of the domain-wall with vector potential $A_a = \pm BW/2$ must be generated by the interaction of the domain wall end density with the electric field at the domain-wall. Because the dominant ground state contribution to the momentum is from the vector potential, the rate of change of canonical momentum (i.e. effective force) amounts to the difference of currents entering the top and bottom edge that must then balance against the electrostatic force, i.e.

$$\begin{aligned} & \left(\mu_- + \frac{j}{2\nu_-} - \phi_t(s=0) \right) \nu_- - \left(\mu_+ + \frac{j}{2\nu_+} - \phi_b(s=0) \right) \nu_+ \\ & = \left(\mu_+ - \frac{j}{2\nu_+} - \phi_b(s=0) \right) \nu_+ - \left(\mu_- - \frac{j}{2\nu_-} - \phi_t(s=0) \right) \nu_- + \sum_{a=t,b} Q_a \phi'_a(s=0), \end{aligned} \quad (7)$$

where we have used the chemical potential notation of Fig. 3 together with Eq. 3 and $Q_{t,b}$ are the charges at the top and bottom ends of the domain-wall. The terms $\phi_{t,b}(s=0)$ are the electrostatic potentials at the top and bottom ends of the domain wall in Fig. 3. The average of the top and bottom potentials are:

$$\frac{\phi_t(s=0) + \phi_b(s=0)}{2} = \frac{\mu_+\nu_+ - \mu_-\nu_-}{\nu_+ - \nu_-} + \sum_{a=t,b} \frac{Q_a \phi'_a(s=0)}{\nu_+ - \nu_-}. \quad (8)$$

The above form motivates us to consider the potential and density in Eq. 6 in a rotated basis where the indices a, b in both Eq. 6 and Eq. 3 refer to symmetric and antisymmetric combinations of the top and bottom edges (i.e. $a, b = S$ and $a, b = A$ respectively). Note that because the Luttinger parameter is the same of the top and bottom edges, this does not modify Eq. 3; however the Coulomb matrix U is rotated from the t, b basis to the S, A basis. The effective chemical potential after this rotation transforms to μ_{\pm} in the symmetric sector and $j/2\nu_{\pm}$ in the antisymmetric sector. Finally, we note that as a matter of principle, Eq. 6 can be solved to obtain both $\phi_{S,A}(s=0)$ and $\phi'_{S,A}(s=0)$ as a function of μ_{\pm} and j . Substituting into Eq. 8 leads to a linear equation in these variables with coefficients $Q_{t,b}$, which are the charges of the domain-wall of the form

$$\left(C_+ + \sum_a D_{+,a} Q_a \right) \mu_+ + \left(C_- + \sum_a D_{-,a} Q_a \right) \mu_- + \left(C_j + \sum_a D_{j,a} Q_a \right) j = \sum_a \int ds F_a(s) \phi_{\text{ext},a}(s), \quad (9)$$

where C_a , $D_{c,a}$ and $F_a(s)$ are functions determined in terms of $U_{ab}(s, s')$ and $\nu_a(s)$. Note that the RHS of the equation does not depend on $\mu_{\pm, j}$ and would drop out of a linear response calculation. Focusing on linear response, this constraint reduces to

$$\left(C_+ + \sum_a D_{+,a} Q_a\right) \delta\mu_+ + \left(C_- + \sum_a D_{-,a} Q_a\right) \delta\mu_- + \left(C_j + \sum_a D_{j,a} Q_a\right) \delta j = 0. \quad (10)$$

Since we cannot (without more microscopic details) determine these charges microscopically, we need to impose a consistency condition that Eq. 8 allows an equilibrium. This would lead to a consistent solution for the equilibrium state $\delta\mu_a = \delta\mu$ for any chemical potential with $\delta j = 0$. This leads to the constraint on the charges

$$\left(C_+ + \sum_a D_{+,a} Q_a\right) + \left(C_- + \sum_a D_{-,a} Q_a\right) = 0. \quad (11)$$

With this constraint Eq. 10 reduces to

$$\left(C_+ + \sum_a D_{+,a} Q_a\right) (\delta\mu_+ - \delta\mu_-) + \left(C_j + \sum_a D_{j,a} Q_a\right) \delta j = 0. \quad (12)$$

Based on Fig. 3, the bias voltage would be

$$\delta V_b = \delta\mu_+ - \delta\mu_- + \delta j \left(\frac{1}{2\nu_+} + \frac{1}{2\nu_-} \right). \quad (13)$$

the conductance would be

$$G = \frac{\delta j}{\delta V_b} \quad (14)$$

$$= \left[\frac{1}{2\nu_+} + \frac{1}{2\nu_-} - (C_j + \sum_a D_{j,a} Q_a)(C_+ + \sum_a D_{+,a} Q_a)^{-1} (\delta\mu_+ - \delta\mu_-)^{-1} \right]^{-1}. \quad (15)$$

Determining the relevant coefficients $C_j, D_{j,a}$ based on Eq. 3, Eq. 6 and Eq. 8 is nontrivial. On the other hand, as mentioned in the main text, it is rather straightforward to solve in the case of a QPC with mirror symmetry. In this case, the equations decouple in the symmetric and antisymmetric (i.e. S and A) sectors with $\delta\mu_{\pm}$ belonging to S and δj belonging to A . Furthermore, symmetry dictates $Q_t = Q_b$, which ensures that Eq. 8 would belong in the sector S . This implies that $C_j = D_{j,a} = 0$. Substituting into the above equation for conductance we get

$$G = \left[\frac{1}{2\nu_+} + \frac{1}{2\nu_-} \right]^{-1}, \quad (16)$$

consistent with the result in the main text.

IMPURITY STRENGTH

We estimate the Luttinger liquid back-scattering parameter g in Eq. 1 in the main text based on the configuration of the QPC in the experiment [12]. In the open junction case, we assume that the 2D electron density interpolates smoothly between $n_{1/3} = 1/2\pi\ell_B^2$ and $n_1 = (1/3)/2\pi\ell_B^2$ over a width L where $\ell_B = \sqrt{\hbar/eB}$ is the magnetic length. From the Supplementary Material of 12, this width is on the order of 100 nm. This gives a background charge gradient $\nabla\rho_0(x) = e/3\pi L\ell_B^2$. Generically, we expect a $\nu = 2/3$ edge mode to develop between these two regimes, which we model as a correction $\delta\rho(x) \propto (x/\ell_B) \exp(-x^2/2\ell_B^2)$ to the density profile. The overall prefactor to this expression is determined by the constraint that $\nabla\rho(x) = \nabla(\rho_0(x) + \delta\rho(x)) = 0$, which leads to

$$\delta\rho(x) = -\frac{ex}{3\pi\ell_B^2 L} \exp\left[-\frac{x^2}{2\ell_B^2}\right]. \quad (17)$$

If this edge mode propagates along the y direction over a width W , the potential at the edge ($y = \pm W/2$) is given by the Greens function of a charged wire

$$G(x) = \log \left[\frac{|x|}{-W + \sqrt{W^2 + x^2}} \right],$$

leading to

$$V(x) = -\frac{1}{4\pi\epsilon} \int_{-\infty}^{\infty} dx' G(x') \delta\rho(x-x'),$$

noting that the potential from ρ_0 is absorbed into the harmonic Luttinger liquid.

Using the results from Ref. 13, the bosonized backscattering parameter g is proportional, at first order, to the Fourier transform of the potential at twice the Fermi momentum $2k_F$. Since the real-space potential is a convolution, the Fourier transform is just a product:

$$\begin{aligned} \tilde{V}(2k_F) &= -\frac{\sqrt{2\pi}}{4\pi\epsilon} \tilde{G}(2k_F) \delta\tilde{\rho}(2k_F) \\ &= -\frac{iek_F\ell_B}{3\pi\sqrt{2\pi}L\epsilon} e^{-2k_F^2\ell_B^2} \tilde{G}(2k_F). \end{aligned}$$

We can approximate $\tilde{G}(2k_F)$ by taking the large W limit in which $G(x) \approx \log|x|$ (up to a constant) and $\tilde{G}(2k_F) = -k_F^{-1}\sqrt{\pi/8}$. Then

$$\tilde{V}(2k_F) = \frac{iel_B}{12\pi L\epsilon} e^{-2k_F^2\ell_B^2}.$$

This expression relates to g as $g \propto a_0^{-1}e\tilde{V}(2k_F)$ where a_0 is the UV cutoff of the bosonization [13]. Therefore

$$g \propto \frac{e^2\ell_B}{12\pi a_0 L\epsilon} e^{-2k_F^2\ell_B^2}.$$

This expression has units of energy, agreeing with the scaling dimension of the boundary sine Gordon model. Note that the a_0 used here and the a in the refermionization section of the main text are not necessarily equal.

Crucially, the Fermi momentum in the quantum hall depends on the spatial separation of the chiral modes. This is due to the magnetic flux through the bulk causing a momentum different between the chiral modes. At the QPC, the shorter width W leads to a lower Fermi momentum. This relationship is quantified as

$$k_F = \frac{\kappa W}{2\ell_B^2},$$

where κ is a factor of proportionality. This form leads g to be exponentially suppressed in width:

$$g \propto \frac{E_C\ell_B^2}{3a_0L} e^{-\kappa^2 W^2/2\ell_B^2}.$$

where $E_C = e^2/4\pi\epsilon\ell_B$ is the Coulomb energy defined in Ref. 12, which in the experimental setup is approximately 37 meV at a magnetic field of 10 T.

In the refermionized expressions for noise and conductance, the impurity is parameterized by a barrier energy $E_B = g^2\pi a/\hbar v$, which becomes

$$E_B \propto \frac{E_C^2 a \ell_B^4}{\hbar v a_0^2 L^2} e^{-\kappa^2 W^2/\ell_B^2}$$

(omitting the $\pi/9$ prefactor). Comparing our results with Ref. 12, the barrier energy relates to T_0 simply as $2E_B = k_B T_0$. The drift velocity v of a skipping state is given as $v = |\nabla V|/B$. Using the definition $E_V = e|\nabla V|\ell_B$ from the Ref. 12 supplementary material, we find $v = E_V\ell_B/\hbar$, leading to

$$E_B \propto \frac{E_C^2 a \ell_B^3}{E_V a_0^2 L^2} e^{-\kappa^2 W^2/\ell_B^2}.$$

In Ref. 12, the junction width is reduced by increasing the north-south gate voltage V_{NS} . The edge state is approximately localized at the point where the drop in potential from the bulk value is equal to the spacing of the Landau levels, given by the cyclotron frequency in graphene [14]

$$\begin{aligned}\omega_c &= \sqrt{\frac{2aev_F^2 B}{\hbar}} \\ &= \sqrt{2} \frac{v_F}{\ell_B}\end{aligned}$$

where $v_F = 1.1 \times 10^6 \text{m/s}$. We model the potential profile as a Gaussian of width W_0 (standard deviation $W_0/2$) in the y direction (North-South in the language of 12). From Fig. S1 we see that this value is on the order of 100nm. The width of the Gaussian at an energy $\hbar\omega_c$ is then

$$\begin{aligned}W &= 2W_0 \sqrt{\log\left(\frac{eV_G}{eV_G - \hbar\omega_c}\right)} \\ &\approx 2W_0 \sqrt{\frac{\hbar\omega_c}{eV_G}}\end{aligned}$$

Plugging this in to our expression for E_B gives

$$E_B \propto \frac{E_C^2 a \ell_B^3}{E_V a_0^2 L^2} \exp\left[-\frac{4\kappa^2 W_0^2 \hbar\omega_c}{eV_G \ell_B^2}\right].$$

Using $E_V \approx eV_G \ell_B W_0/2$, and assuming that W_0 and L are of similar order ($\approx 100\text{nm}$), we find

$$E_B \propto \frac{E_C^2 a \ell_B^2}{eV_G a_0^2 W_0} \exp\left[-\frac{4\kappa^2 W_0^2 \hbar\omega_c}{eV_G \ell_B^2}\right].$$

We can approximate the cutoff a as $L \sim W_0$ since our refermionized picture assumes a sharp crossover between free fermions and we take the standard approximation $a_0 \sim k_F^{-1} = \ell_B^2/W_0$, using W_0 in lieu of W to ensure that this cutoff is constant as we tune V_G . Then,

$$E_B \propto \frac{E_C^2 \kappa^2 W_0^2}{eV_G \ell_B^2} \exp\left[-\frac{4\kappa^2 W_0^2 \hbar\omega_c}{eV_G \ell_B^2}\right].$$

This expression can be simplified by considering two parameters of the experimental system: $W_0/\ell_B \approx 12.3$ and $\hbar\omega_c = \sqrt{2}\hbar v_F/\ell_B \approx 0.126\text{eV}$ at $B = 10\text{T}$.

$$E_B \propto \frac{E_C^2 a \ell_B^2}{eV_G a_0^2 W_0} \exp\left[-\frac{4\kappa^2 W_0^2 \hbar\omega_c}{eV_G \ell_B^2}\right].$$

Then $T_0 = 2E_B/k_B$ used in Ref. 12 follows the general form

$$T_0 \propto \frac{A}{V_{\text{EW}} - V_{\text{NS}}} e^{-V_0/(V_{\text{EW}} - V_{\text{NS}})}$$

where $A = \kappa^2 E_C^2 (W_0/\ell_B)^2 / 2ek_B \approx 10^3 \kappa^2 \text{K} \cdot \text{V}$ and $V_0 = 4\kappa^2 (W_0/\ell_B)^2 (\hbar\omega_c)/e \approx 10^2 \kappa^2 \text{V}$, substituting $V_G = V_{\text{EW}} - V_{\text{NS}}$.

This functional form generally matches the relationship between T_0 and V_{NS} found in Ref. 12, resembling an exponential in a neighborhood of V_{NS} . The general scale can be made to fit with an appropriate choice of κ . Since this proportionality factor occurs squared in the exponential, it has a large effect on the scale of T_0 .

Connecting to spin-chain numerics

We also want to relate E_B to the spin-chain impurity u used in the numerical simulations found in the main text. This impurity acts on a single site, giving a Fourier-transformed potential of

$$\tilde{V}(k) = \sqrt{\frac{2}{\pi}} \frac{u \sin(ka_0/2)}{k}$$

where a_0 is the lattice constant. To calculate the sine-Gordon impurity g , we evaluate this at $k_F = \pi n/a_0$ where n is the 1D per-site occupancy (measured to be approximately 0.7 particles per site in our simulations). This gives a barrier energy of

$$E_B = \frac{au^2 \sin^2(\pi n)}{2\pi^2 n^2 v}.$$

Using the known velocity of $v = 0.5$, this expression shows a quadratic relationship between E_B with a prefactor on the order of 10^{-1} , assuming the refermionized cutoff a to be on the order of 1 lattice site.

We see this quadratic relationship in Fig. 2(bottom) of the main text, which yields a prefactor of 0.55. This value is roughly the same order as expected.

LEADS AT DIFFERENT TEMPERATURES

An interesting extension of our analysis occurs when the leads are at different temperatures T_{\pm} , which results in a non-Fermi distribution for the $\psi(x)$ fermion given by the modified Fermi distribution $\tilde{n}_F(k)$. This distribution is derived from noting that ψ_c is an exponential of ξ and therefore also of ϕ_{\pm} and observing that these bosonic fields have Gaussian distribution.

The effective fermion field ψ_c is expressed in terms of the chiral boson field $\xi_c(x)$, which relates to the original chiral fields as

$$\xi_c(x) = \frac{\Gamma}{\sqrt{K_-}} \phi_{-,c}(x) + \frac{\Gamma}{\sqrt{K_+}} \phi_{+,c}(x)$$

where

$$\phi_{\pm,c}(x) = \frac{1}{2} \left[K_{\pm}^{-1/2} \phi_{\pm}(x) + K_{\pm}^{1/2} \int_0^x dx' \Pi_{\pm}(x') \right].$$

Using the canonical commutation relation $[\phi(x), \Pi(x')] = i\pi\delta(x-x')$ and the folded field definitions $\phi_{\pm}(x) = \phi(\pm x)$ and $\Pi_{\pm}(x) = \Pi(\pm x)$, we can show that the two chiral fields $\phi_{+,c}$ and $\phi_{-,c}$ commute with each other (though not with themselves at differing x). Therefore, products of effective fermions separate as

$$\begin{aligned} \langle \psi_c^\dagger(x_1) \psi_c(x_2) \rangle &= \langle e^{2i\xi_c(x_1)} e^{-2i\xi_c(x_2)} \rangle \\ &= \langle e^{(2\Gamma/\sqrt{K_+})i\phi_{+,c}(x_1)} e^{-(2\Gamma/\sqrt{K_+})i\phi_{+,c}(x_2)} \rangle \langle e^{(2\Gamma/\sqrt{K_-})i\phi_{-,c}(x_1)} e^{-(2\Gamma/\sqrt{K_-})i\phi_{-,c}(x_2)} \rangle, \end{aligned}$$

assuming that far from the impurity $\phi_{-,c}$ and $\phi_{+,c}$ are independent. Using the property of bosonic operators that $\langle \exp[\lambda \hat{B}] \rangle = \exp[\lambda^2 \langle \hat{B}^2 \rangle / 2]$, we calculate

$$\begin{aligned} \langle \psi_c^\dagger(x_1) \psi_c(x_2) \rangle &= e^{-4\Gamma^2/K_+ \langle \phi_{+,c}(x), \phi_{+,c}(x') \rangle / 2} e^{-4\Gamma^2/K_+ \langle (\phi_{+,c}(x_1) - \phi_{+,c}(x_2))^2 \rangle} \times (+ \iff -) \\ &= \langle e^{2i\phi_{+,c}(x_1)} e^{-2i\phi_{+,c}(x_2)} \rangle^{\Gamma^2/K_+} \langle e^{2i\phi_{-,c}(x_1)} e^{-2i\phi_{-,c}(x_2)} \rangle^{\Gamma^2/K_-} \\ &= \langle \psi_+^\dagger(x_1) \psi_+(x_2) \rangle^{\Gamma^2/K_+} \langle \psi_-^\dagger(x_1) \psi_-(x_2) \rangle^{\Gamma^2/K_-}. \end{aligned} \quad (18)$$

where $\psi_{\pm}(x) = \exp[2i\phi_{\pm}(x)]$. If ψ_{\pm} is described by a Fermi-Dirac distribution n_F with temperature T_{\pm} , these correlators are given by the Fourier transform of $n_F(k)$:

$$\langle \psi_{\pm}^\dagger(x+r) \psi_{\pm}(x) \rangle = -\frac{i\pi T_{\pm}}{\sinh \pi T_{\pm} x}$$

assuming translation invariance far from the boundary. Using this expression and Eq. 18, we find an effective distribution

$$\begin{aligned} \tilde{n}_F(k) &= \int dx e^{ikx} \left(\frac{-i\pi T_+}{\sinh \pi T_+ x} \right)^{\Gamma^2/K_+} \left(\frac{-i\pi T_-}{\sinh \pi T_- x} \right)^{\Gamma^2/K_-}, \\ &= \int_0^\infty dx \sin(kx) \Phi(x), \end{aligned} \quad (19)$$

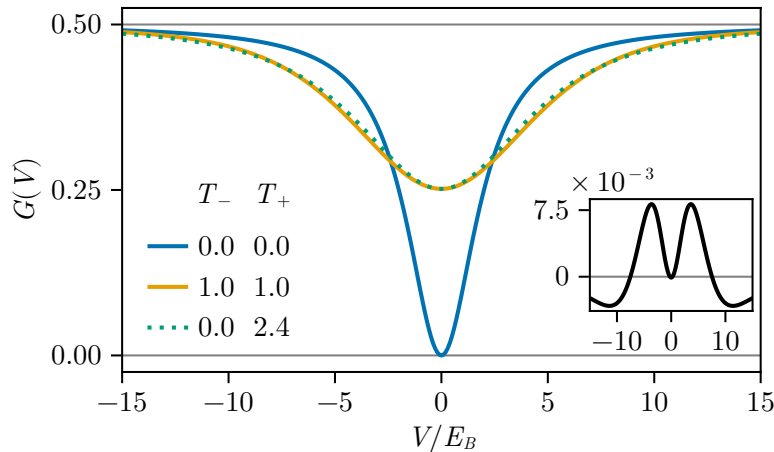


FIG. 2. Voltage-dependent conductance for various temperatures demonstrating approximate equivalence between asymmetric and symmetric lead temperatures. Inset shows absolute difference between $T_- = 0$, $T_+ = 2.4$ conductance and $T_- = 1.0$, $T_+ = 1.0$.

where

$$\Phi(x) = \left(\frac{T_+}{\sinh \pi T_+ x} \right)^{\Gamma^2/K_+} \left(\frac{T_-}{\sinh \pi T_- x} \right)^{\Gamma^2/K_-}.$$

This formula reduces to the Fermi distribution for $T_- = T_+$.

The current, conductance and shot noise can now be computed by simply substituting \tilde{n}_F for n_F . For the conductance, we can use the Eq. 11 from the main text to get

$$G(V) = \frac{e^2}{2h} \left(1 - \frac{E_B}{2} \int_0^\infty dx x \Phi(x) e^{-E_B x \cos(V/2)x} \right).$$

We plot the results of this function, numerically integrated with a Gauss-Kronrod quadrature formula, in Fig. 2. The result shows a small difference in the conductance when the leads are at different temperatures compared to the conductance with an effective single temperature.

-
- [1] V. Zauner-Stauber, L. Vanderstraeten, M. T. Fishman, F. Verstraete, and J. Haegeman, *Physical Review B* **97**, 045145 (2018).
 - [2] R. Vlijm, M. Ganahl, D. Fioretto, M. Brockmann, M. Haque, H. G. Evertz, and J.-S. Caux, *Physical Review B* **92**, 214427 (2015).
 - [3] M. Ganahl, E. Rabel, F. H. Essler, and H. G. Evertz, *Physical review letters* **108**, 077206 (2012).
 - [4] J. Von Delft and H. Schoeller, *Annalen der Physik* **510**, 225 (1998).
 - [5] C. d. C. Chamon and E. Fradkin, *Physical Review B* **56**, 2012 (1997).
 - [6] N. P. Sandler, C. d. C. Chamon, and E. Fradkin, *Physical Review B* **57**, 12324 (1998).
 - [7] N. P. Sandler, C. d. C. Chamon, and E. Fradkin, *Physical Review B* **59**, 12521–12536 (1999).
 - [8] B. Muzykantskii and D. Khmelnitskii, *Physical Review B* **50**, 3982 (1994).
 - [9] M. De Jong and C. Beenakker, *Physical Review B* **49**, 16070 (1994).
 - [10] C. Kane, M. P. Fisher, and J. Polchinski, *Physical review letters* **72**, 4129 (1994).
 - [11] A. M. Chang, *Reviews of Modern Physics* **75**, 1449 (2003).
 - [12] L. A. Cohen, N. L. Samuelson, T. Wang, T. Taniguchi, K. Watanabe, M. P. Zaletel, and A. F. Young, *Science* **382**, 542 (2023).
 - [13] C. Kane and M. P. Fisher, *Physical Review B* **46**, 15233 (1992).
 - [14] L.-J. Yin, K.-K. Bai, W.-X. Wang, S.-Y. Li, Y. Zhang, and L. He, *Frontiers of Physics* **12**, 10.1007/s11467-017-0655-0 (2017).